An intermediate-scale model for thermal hydrology in low-relief permafrost-affected landscapes

Ahmad Jan[a,*], Ethan T. Coon[b], Scott L. Painter[a], Rao Garimella[c], J. David Moulton[c]

[a] *Climate Change Science Institute and Environmental Sciences Division, Oak Ridge National Laboratory, Oak Ridge, Tennessee, USA*
[b] *Computational Earth Sciences Group, Earth and Environmental Sciences Division, Los Alamos National Laboratory, Los Alamos, New Mexico, USA*
[c] *Applied Mathematics and Plasma Physics Group, Theoretical Division, Los Alamos National Laboratory, Los Alamos, New Mexico, USA*

Abstract

Integrated surface/subsurface models for simulating the thermal hydrology of permafrost-affected regions in a warming climate have recently become available, but computational demands of those new process-rich simulation tools have thus far limited their applications to one-dimensional or small two-dimensional simulations. We present a mixed-dimensional model structure for efficiently simulating surface/subsurface thermal hydrology in low-relief permafrost regions at watershed scales. The approach replaces a full three-dimensional system with a two-dimensional overland thermal hydrology system and a family of one-dimensional vertical columns, where each column represents a fully coupled surface/subsurface thermal hydrology system without lateral flow. The system is then operator split, sequentially updating the overland flow system without sources and the one-dimensional columns without lateral flows. We show that the approach is highly scalable, supports subcycling of different processes, and compares well with

*Corresponding Author: Ahmad Jan; Email: jana@ornl.gov; Phone: (865) 576-8175.

the corresponding fully three-dimensional representation at significantly less computational cost. Those advances enable recently developed representations of freezing soil physics to be coupled with thermal overland flow and surface energy balance at scales of 100s of meters. Although developed and demonstrated for permafrost thermal hydrology, the mixed-dimensional model structure is applicable to integrated surface/subsurface thermal hydrology in general.

Keywords: Multiscale models, Permafrost thermal hydrology, Integrated surface/subsurface flow modeling, Arctic

---

1. Introduction

Approximately 23% of the land surface in the Northern Hemisphere is underlain by continuous permafrost (91-100% frozen area), and another 17% is occupied by discontinuous permafrost (50-90% frozen area) [1, 2]. A massive amount of organic carbon is stored in those regions [3, 4], which are warming at a rate considerably faster than the rest of the planet [5, 6, 7]. As the soils in that region warm, they have the potential to transform from a net sink to a net source of carbon to the atmosphere, which could increase the concentration of carbon in the atmosphere and in turn lead to further increase in the temperature (e.g. [8]). Further, thawing and the resulting degradation of permafrost can cause significant changes in the surface and subsurface thermal hydrology and eventually can substantially alter the Arctic tundra ecosystems [9, 10, 11, 12, 13].

Those potential impacts and feedbacks in the terrestrial Arctic have motivated the development of increasingly sophisticated tools for simulating permafrost dynamics in a warming climate. Such simulations can help to

better understand the consequences of soil warming and responses of tundra ecosystems to warming trends, and further expose the effects of permafrost degradation on surface and subsurface thermal hydrology. However, simulating permafrost dynamics in a complex and coupled surface/subsurface thermal hydrological environment is a challenging task, especially at larger spatiotemporal scales [14]. A comprehensive review of the modeling efforts of the surface and subsurface can be found in [15]. Early research efforts focused on one-dimensional simulations for fundamental understanding of infiltration in cold climates; see, for example, [16, 17, 18]. Similar one-dimensional approximations have been adopted as coarse-scale models in global land surface models [19, 20, 21, 13]. Two-dimensional simulations with simplified physics (i.e. saturated conditions, subsurface only) have been used for understanding evolution of field-scale groundwater systems [22, 23], but do not represent key unsaturated zone processes that are needed to understand active layer dynamics and decomposition of soil organic matter. It is worth pointing out that mathematical models with limited complexity, reduced dimensionality, and relatively coarse spatial resolutions provide some insight into permafrost dynamics but fail to represent important processes such as cryosuction, lateral surface and subsurface flows, and advective heat transfers. Simulations with more mechanistic representations of surface and vadose zone process in three-dimensions are essential to accurately capture the potential impacts of permafrost thawing on the surface and subsurface thermal hydrology and the resulting effects on the carbon cycle.

Two- and three-dimensional models with explicit physics-based representations of ice/liquid/gas partitioning in the vadose zone have only recently started to appear [24]. Painter [25] developed the three-phase, two-component model MarsFlo which has been used in Mars [26] and Earth

permafrost studies [27]. Karra et al. [28] simplified that subsurface freezing-soil thermal hydrology representation by ignoring gas advection and implemented that Richards-like approximation in the highly parallel PFLOTRAN [29] code. Kumar et al. [30] used that implementation in three-dimensional microtopography-resolving thermal hydrology simulations of polygonal tundra. Those computer codes are all subsurface-only models; that is, they do not represent surface flows and surface energy balance. Painter et al. [31] recently introduced the Arctic Terrestrial Simulator, which uses a sophisticated multiphysics management framework [32] to couple the three-dimensional subsurface representation of [28] with a two-dimensional non-isothermal surface flow model, surface energy balance with and without snow, and a simple snow distribution model.

Despite the significant progress in developing integrated surface/subsurface permafrost thermal hydrology models, significant challenges remain in moving to climate-relevant spatiotemporal scales. One of the challenges is that the integrated system is numerically stiff because of the highly dynamic surface system [31] and the ice-liquid phase transition [33], which often results in relatively small time steps to achieve convergence. Small time steps are not problematic in one-dimensional simulations because a well-designed simulation tool will recover the time step quickly after a convergence failure. However, a small time step becomes problematic in large three-dimensional runs because it becomes increasingly likely that, at any given time, at least one computational cell will be experiencing a phase change and thus a small time step. The other major challenge is tracking thaw-induced subsidence. Traditional hydrological simulators are mainly designed to conduct three-dimensional simulations, however, deformations in a three-dimensional simulation are not easy to track due to mesh tangling and can be computation-

ally expensive; further, poor mesh quality may raise questions about the accuracy of the results.

To address the aforementioned challenges, we present a mixed-dimensional modeling strategy for process-rich simulations of integrated surface and subsurface thermal hydrology in tundra systems with low topographic gradients. The approach is intended for spatial scales intermediate between microtopography-resolving fine-scale simulations and the scale of an Earth system model grid cell. We demonstrate with simulations of polygonal tundra, large and carbon-rich regions of northern Siberia, Alaska, and Canada where soil cracking has led to the formation of subsurface ice wedges that honeycomb the subsurface and tessellate the land surface into polygonal patterns. Rather than solve a fully three-dimensional subsurface system tightly coupled to surface processes as in [31], we take advantage of physical insights gained from fine-scale simulations and approximate the integrated surface/subsurface dynamics with mutually independent 1-D columns, each associated with an ice wedge polygon. The columns are then sequentially coupled to a surface thermal flow system, solving the surface problem in an operator-split manner. This mixed-dimensional modeling approach is motivated by fine-scale simulations at the ice-wedge polygon scale that showed that differences in the thermal conditions among centers, rims and troughs of ice-wedge polygons are largely equilibrated by lateral heat transport during summer such that the system behaves similarly to a one-dimensional system on seasonal time scales. Mixed-dimensional model structures have been used previously in simulations of variably saturated flow at watershed scales, in particular to couple multiple 1-D unsaturated (vadose) zone representations to a two- or three-dimensional saturated zone; for example see [34, 35, 36]. Here we apply the mixed-dimensional model structure to an

integrated surface/subsurface flow system including surface and subsurface thermal processes and evaluate the accuracy and computational advantages of the approximation.

The paper is organized as follows: Section 2 highlights the Advanced/Arctic Terrestrial Simulator (ATS) and the Arcos multiphysics management framework, within which we implemented our approach. Section 3 presents some fine-scale simulation results and analysis that motivated the approach. In Section 4 we introduce our mixed-dimensional modeling approach, loosely coupled scheme and the ATS refactoring strategy. To illustrate the performance and efficiency of our modeling strategy, in Section 5 we compare our numerical results with the three-dimensional simulations based on strong coupling, and present speedup and scalability of the new technique. Concluding remarks and future research are offered in Section 6.

2. The ATS Software

We implemented our mixed-dimensional modeling strategy in open-source parallel software known as Amanzi-ATS [37] (or simply ATS). Amanzi-ATS is the result of extending the flow and reactive transport simulator Amanzi [38] by adding an advanced multiphysics management system known as Arcos [32]. Arcos is key to managing the complex spatial structures used here. It was originally built to manage couplings among process models (denoted process kernels and abbreviated as PKs), which may be selected at runtime. A PK encapsulates the mathematical representation of a particular physical process or coupled set of processes; PKs are coupled together through Multiprocess Coordinators MPCs. An MPC is regarded as a PK by MPCs at higher levels in the tree, thus allowing complex hierarchical model

structures to be built dynamically at runtime. In this work, we used Arcos to coordinate not only process kernels but also subdomains of the larger spatial domain.

Amanzi, and by extension ATS, uses the Trilinos [39] framework for parallel infrastructure. An unstructured mesh framework [40] is included for interacting with the computational mesh. General polyhedral meshes are supported. Discretization accuracy is maintained on the potentially distorted grids through the use of the mimetic finite difference (MFD) method [41, 42]. The backward Euler method is used for time stepping with a Nonlinear Krylov Acceleration (NKA) method [43, 44] to solve the resulting discretized residual equations.

The initialism ATS may refer to either the Advanced Terrestrial Simulator, which is the general capability, or the Arctic Terrestrial Simulator, which is one particular configuration [31], depending on context. The Arctic Terrestrial Simulator configuration solves strongly coupled surface energy balance, and surface and subsurface thermal hydrology with freeze/thaw dynamics. This work extends the ATS to work with a multicolumn spatial structure.

3. Motivation: Results from Fine-scale Simulations

This mixed-dimensional approach is motivated by the results of fine-scale, two-dimensional simulations on vertical cross-sections across ice-wedge polygons at the Barrow Environmental Observatory. The simulations coupled a surface energy balance model potentially including snow, snow distribution models, models for thermal overland flow including phase change, and a recently developed three-phase subsurface thermal hydrology model.

The soil properties were calibrated against borehole temperature data in a previous study [45]. The simulations were forced with meteorological data for the site. Those simulations used an unstructured mesh that conforms to surface topography derived from lidar measurements. Horizontal mesh resolution is approximately 0.25 m. Vertical resolution is 0.02 cm at the surface and gradually increases with depth. Details on boundary conditions and the spinup process can be found in [31].

Snapshots of ice and liquid saturation indices in cross-section across two ice-wedge polygons are shown in Fig. 1. These snapshots are for October 15, 2013, which is during the fall freeze-up. During this period, the rims of the ice-wedge polygons are significantly colder than the centers and troughs because the thermally insulating snowpack is smaller on the rims. Previous one-dimensional simulations [46] have shown that thermal differences caused by differences in snow depth lead to differences in active layer thickness, the depth of the annual thaw. However, in the two-dimensional simulations shown here, the active layer thickness shows little variation across the polygon (Fig. 2). Although transient differences in subsurface temperature occur due to differences in snow depth, soil moisture content, and albedo, lateral heat transport is sufficient to equilibrate those differences by the time of maximum thaw. Thus, the active layer thickness, which is a primary control on the annual carbon decomposition rates, is not directly affected by microtopographic position within an ice-wedge polygon in cases where organic matter is relatively uniform. This lack of sensitivity suggests a model structure where the ice-wedge polygon becomes the unit computational cell on the surface.

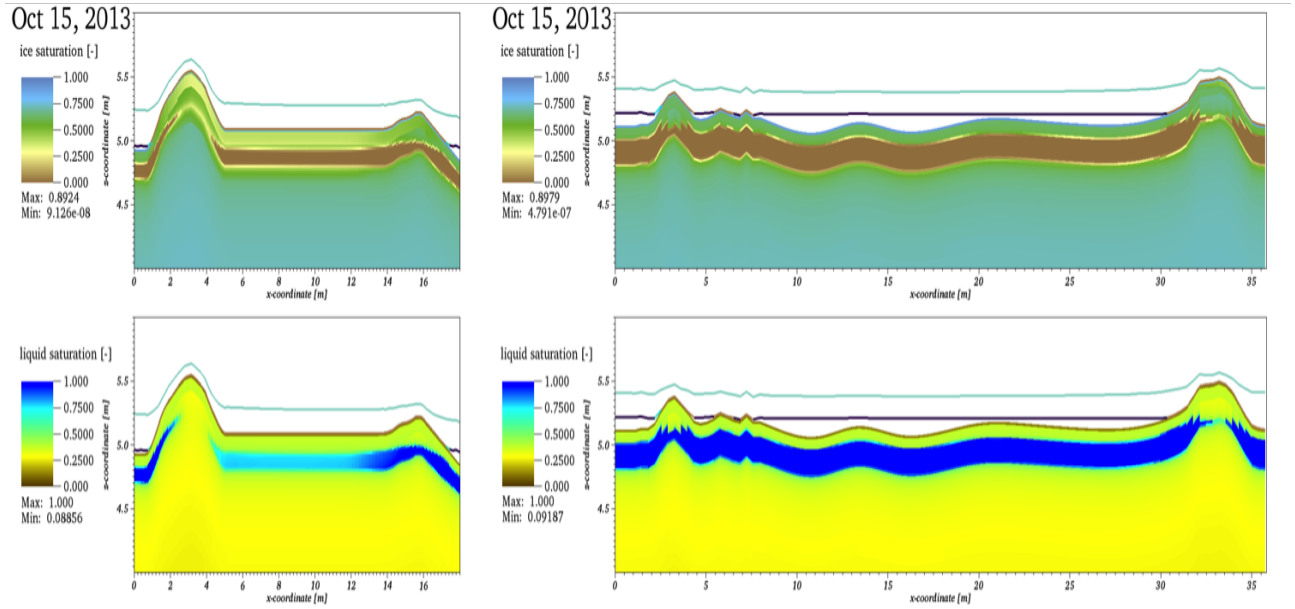

Figure 1: Results from two-dimensional fine-scale modeling. Shown are snapshots of ice saturation index and liquid saturation index in cross-sections across two ice-wedge polygons.

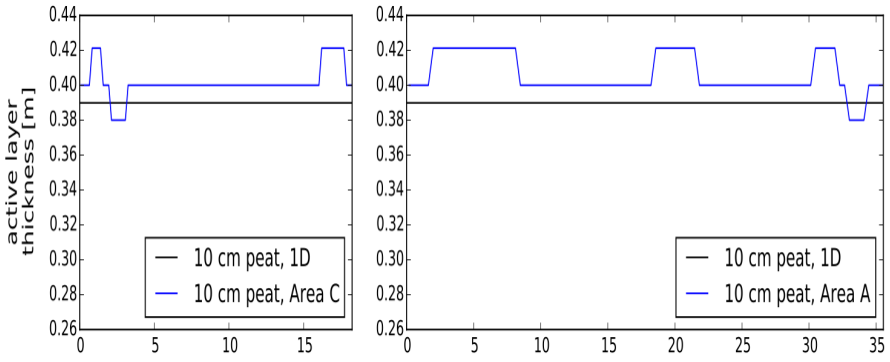

Figure 2: Active layer thickness from fine-scale modeling. Note that the mesh resolution here is $2cm$, and the discontinuities reflect jumps between cells of the mesh.

4. An Intermediate-scale Model

Recognizing the lack of sensitivity to lateral, subsurface flow described above, we propose an intermediate-scale model to leverage this simplification. This model has two components: a spatial structure that combines one-dimensional and two-dimensional domains, and an operator splitting scheme that decouples the columns by solving lateral flow on the surface system independently of the sources and sinks of mass and energy which couple the surface and subsurface systems. We describe those aspects in this section, followed by a discussion of the refactoring strategy used to implement this model within the ATS.

4.1. Mixed-Dimensional Modeling Approach

To build an intermediate scale model, we first tessellate the land surface into N surface cells, where each cell in the surface mesh corresponds to an ice-wedge polygon. Custom mesh generation tools are then used to construct a 3D mesh by extruding each of the surface polygons vertically into

the subsurface, honoring soil layering structure. This 3D mesh represents the entire domain of interest and is referred to as the primary mesh. For the purpose of this model, each tessellated ice-wedge polygon, along with the volume of soil directly below it, is extracted as a single, one-dimensional (in the z-direction) column. On each column, vertical flow of mass and transport of energy are solved, allowing for ponding of water and accumulation of associated energy on each column's surface. A surface balance is also performed on each column's surface to determine the net source of mass and energy into the system. We note that strong (implicit) coupling of the surface, subsurface, and surface energy balance are critically important for accuracy and stability of the system in the presence of strong nonlinearities; this is imposed by solving each column as an integrated system that includes a surface cell in addition to the soil below. The columns are then coupled through lateral surface flow, which quickly moves water and energy throughout the domain.

4.2. Operator Splitting Scheme

Due to the need for strong coupling between the surface and subsurface, the above mixed-dimensional strategy would, by itself, still result in a computationally expensive system of equations that solves all the columns and the surface flow equations simultaneously. To reduce that computational burden, we developed a two-stage operator-split strategy for the surface flow and energy equations. Under this strategy, we split the lateral fluxes from the coupling fluxes, first advancing one and then the other. In the first stage of the splitting, lateral fluxes are allowed to redistribute water and energy across the surface domain with no sources or sinks. This stage is hereafter called the "overland system." Then, in a second update, the

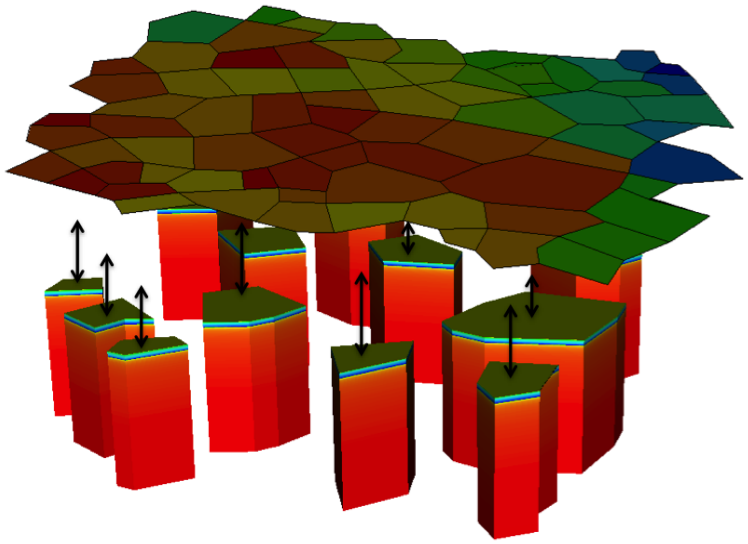

Figure 3: An illustration of the independent 1D columns coupled to the overland system. Although shown here as a subsurface system only, each column also includes a single surface cell with the soil column, and is coupled to a surface energy balance calculation.

coupling fluxes and columnar subsurface are solved implicitly, but independently of every other column. Each column consists then of the subsurface thermal hydrology, surface energy balance, and surface ponding and energy exchange fluxes with no lateral flow. This stage is hereafter called the "column system." This splitting is shown schematically in Fig. 4. For the sake of clarity, we will refer to the pressure and temperature fields after the first stage as "overland-flow" pressure and temperature, while those after the second step will be called "subsurface" and "column-surface" pressures and temperatures. The splitting scheme conserves mass and energy but introduces splitting error, which is quantified through numerical experiments below.

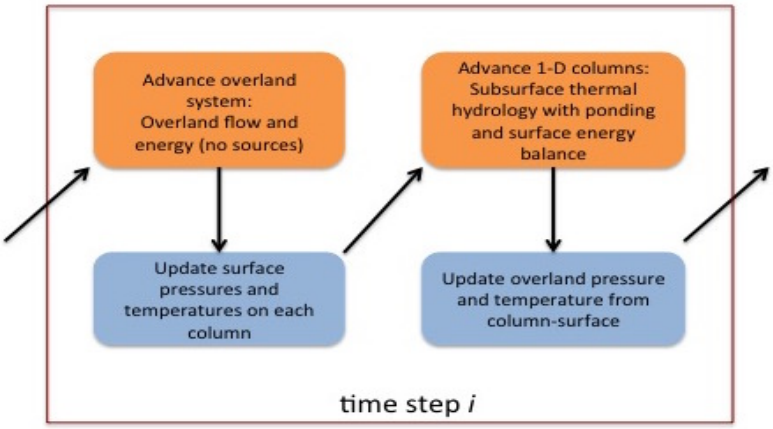

Figure 4: Schematic of the operator splitting scheme for our mixed-dimensional model.

4.3. Model Implementation with ATS and Arcos

This implementation of this strategy requires significant software infrastructure and refactoring support. First, and not trivially, physics and simulation data must be entirely modular and encapsulated, so that multiple

instances of each physics process can be instantiated, allowing separate solution on multiple domains. Next, coupling these many processes on many domains requires a flexible, hierarchical coupling framework. Much of this was supported by Amanzi-ATS's multiphysics library, Arcos. A brief overview of the Arcos framework is provided in section 2, for more details see [32]. Arcos represents physics on these domains as a hierarchical Process Kernel (PK) tree which shows how the processes are coupled on and across these domains, as illustrated in Fig. 5. The PK tree consists of individual conservation equations (for example, the diffusion wave equation for overland flow), strong (globally implicit) couplers, and weak (sequential) couplers highlighted in blue, light cyan, and orange colors, respectively. In our approach, the operator splitting between the overland and column-surface systems happens at the top level weak MPC. As discussed earlier, an MPC is a Multiprocess Coordinator which manages coupling among PKs. The strong MPC (on the left at the second level) is the overland system; the weak MPC at the second level iterates over all the column subdomains. The PK-I, I $= 1, 2, 3, \ldots, N$ denote an integrated system composed of surface energy balance, column-surface (a single cell for coupling fluxes) and subsurface (1D column) system. The tree attached to the black octagon shape is replicated across all PK-I, I $= 1, 2, 3, \ldots, N$.

Refactoring of both ATS and its use of Arcos were needed to implement this strategy. To manage data encapsulation and replication, Arcos's state object stores a dynamic, runtime-determined set of simulation data. Each data is identified by a unique key, e.g. "ponded_depth", and a set of metadata including domain of applicability, mesh entity, number of degrees of freedom, etc. In order for each PK to be instantiated multiple times, that PK's data was altered to enforce uniqueness of its keys by prefixing a do-

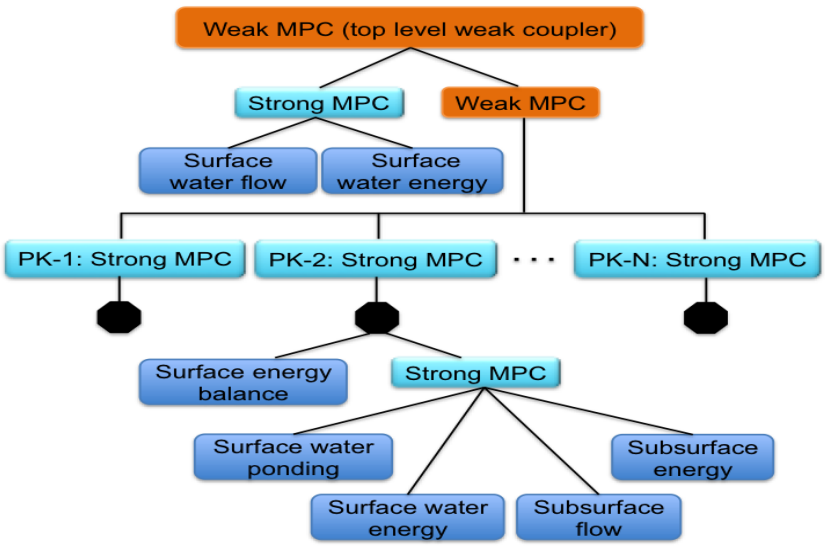

Figure 5: A customized hierarchical structure of the process kernels. Blue blocks highlights independent process kernels; Light blue blocks strongly coupled independent process kernels; Orange blocks represent weak couplers. Multiprocess Coordinator (MPC) highlighted by the light blue blocks couple the lower level PKs. A Process Kernel in the lower levels represents a single partial differential equation.

main identifier such as "column_0_surface-ponded_depth". This refactoring allows multiple instances of any given PK, each attached to a different mesh representing a subdomain of the primary mesh.

Furthermore, Amanzi-ATS relies on a meshing infrastructure, MSTK, [40] which can generate meshes as subdomains or subsets of existing meshes. This framework was extended to allow column meshes to be generated from an existing three-dimensional mesh. In this workflow, a surface mesh consisting of the surface polygons are extruded vertically, following pre-determined soil horizon structure, to create a 3D mesh. By insisting that the extrusion process works only in the vertical, well-defined columns then exist in the the three-dimensional mesh. At run-time, columns can then be identified, and extracted to form a one-dimensional mesh. This mesh is altered to ensure it is a one-dimensional submanifold of three-dimensional space, i.e. each cell has two faces, and all face-normals are $\pm\hat{z}$. Once this is done, Amanzi-ATS's existing operators can work on this mesh without changes. Furthermore, this mesh follows polygonal ground, and therefore consists of stacked polygonal-prisms. Few mesh and visualization libraries or utilities support this fully-unstructured mesh type; a Silo[47] capability was added to to Amanzi-ATS's existing output options to enable visualization of the resulting solution.

Each of these refactors was accomplished in reasonable time thanks to a close adherence to computational software best practices. A series of unit and regression tests were added for each new capability, and the existing regression tests were updated with the domain prefixes. Version control enabled close collaboration on this process across multiple developers, and project-management Kanban tools were used to ensure each developer in the workflow knew the needs of the client code component. These best

practices, along with the use of libraries such as Silo, MSTK, and Arcos, greatly improved the efficiency of what otherwise would have been a difficult development effort.

5. Results and Discussions

In this section, we present numerical results that highlight the accuracy and efficiency of our modeling technique. At the development stage, several numerical experiments were performed to verify the physical behavior of the refactored modules (PKs) of the ATS, code verification details are presented in Appendix A. The spinup process (i.e., model's initialization) has been described in detail in [31].

5.1. Numerical Results – A Comparative Study

To demonstrate the accuracy of our modeling technique, we compare numerical results of the mixed-dimensional model against a fully coupled three-dimensional simulations that act as a benchmark for our simulations. The domain under consideration has surface elevation varying between 4.14-4.62 m, is 40 m deep, and enclosed by a rectangle in the horizontal plane 173×160 m^2; see Fig. 6. This domain is a part of the low-gradient polygonal tundra in Barrow, Alaska and consist of 75 ice wedge polygons. As highlighted in Fig. 6, we select five spots (based on different elevations) to perform a location-based comparison of the numerical results of the two schemes.

In addition to evaluating the quality of our mixed-dimensional approach for the Barrow tundra, we also want to understand when it will give inaccurate results. Because our modeling strategy is based on a loosely coupled scheme and neglects subsurface lateral flow between ice wedge polygons, it

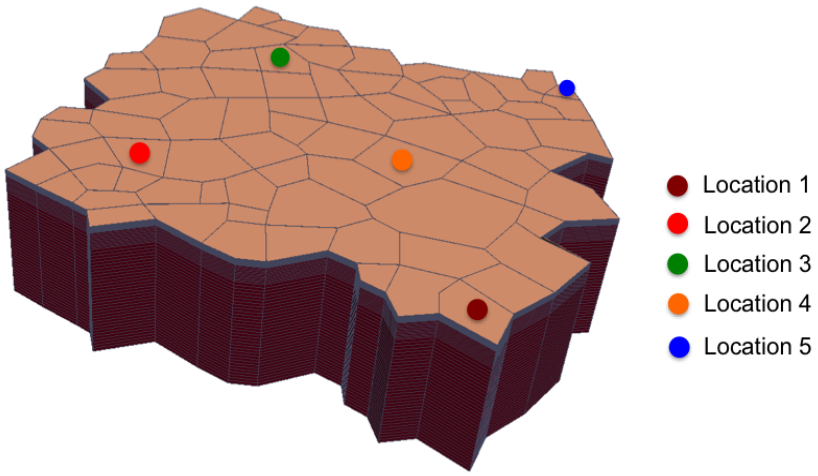

Figure 6: An illustration of the five spatial locations on 75 polygons cluster for location-based comparison of the two schemes. Location 1: Outlet. Location 2: High elevated spot. Location 3-4: Intermediate elevation spots. Location 5: Low elevation spot.

should eventually become inaccurate if the topographic relief is sufficiently large. To identify the range of applicability, we consider three variants of the surface topography. We use the following equation to exaggerate the surface topography,

$$\bar{Z} = \alpha(Z - \mu) + \mu. \tag{1}$$

Here $\bar{Z}$ is the exaggerated elevation, Z is the original elevation with mean μ, and α is the exaggeration parameter. Equation (1) preserves the mean while the standard deviation depends on the value of α and is given in meters by 0.14α. The coefficient in front of α is the standard deviation of the original elevation Z – in our case Z correspond to the domain shown in Fig. 6. Our three variants correspond to $\alpha = 1, 3$, and 5. The value $\alpha = 1$ corresponds to the original topography with slope (between the highest and lowest elevation spots) of 0.37%. The slope increases from 0.37% to 1.1%

and 1.85% for $\alpha = 3$, and 5, respectively. We expect the model to give promising results for simulating low-gradient polygonal tundra, and believe that the values of α we choose provide sufficient variation across a domain of 100s of meter.

Our numerical experiments confirm a high agreement between the results of the mixed-dimensional model and the 3D model at all selected location for all three α values. Figs. 7 and 8 compare the subsurface water saturations and temperatures, respectively, at locations 1 and 5 and for $\alpha = 1$. The accuracy of our results for the Barrow topography ($\alpha = 1$) is evident. The surface ponded depths and temperatures obtained with the two models are depicted in Fig. 9 and 10, respectively. As expected, our results fit the 3D model's results very well. We see the same level of agreement at the other locations as well, but we are not showing them here. In Fig. 11 we plot the mean annual thaw depth at five locations for the three variants, $\alpha = 1, 3$, and 5. We use the annual mean of the thaw depth rather than the maximum thaw depth (i.e. the active layer thickness) because the mean annual thaw depth depends on both the duration of thaw and maximum thaw depth. Thus it is a direct measure of soil available for decomposition, averaged over the year. Not surprisingly, as the value of α increases the mean annual thaw depth deviates from the results of the 3D model to some extent, but we still see the results of the mixed-dimensional model agree well with the corresponding benchmark solution. The annual thaw depth is mainly determined by heat input to the subsurface during the summer season with a very limited memory effect from the previous year. Thus, we do not expect errors in the annual thaw depth to accumulate year to year.

The consistency of our numerical results with the fully coupled 3D simulations confirm the appropriateness of the approximate scheme. As with any

splitting scheme, accuracy and numerical performance will depend on the time step size. Results shown here were obtained with an adaptive time step determined by the minimum preferred time step for surface and subsurface PKs.

Lastly, for demonstration purpose only, the surface ponded depth and temperature during the snowmelt in 2012 are presented in Fig. 13 for the 468 polygon domain. Fully coupled 3D simulations at such a scale are computationally very expensive.

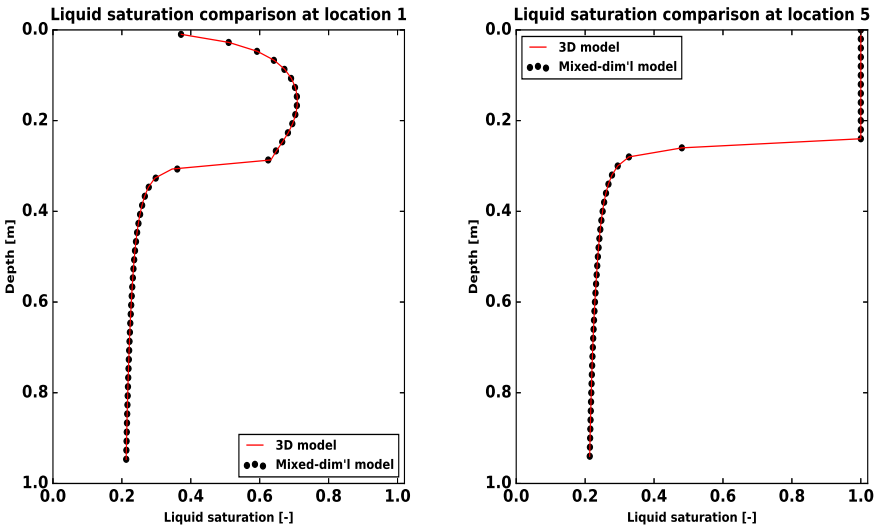

Figure 7: Comparison of the subsurface liquid saturation at locations 1 and 5 during the summer. Results correspond to $\alpha = 1$.

5.2. Speedup Study

We discuss speedup and parallel efficiency for two spatial domains, one with 75 polygons (see Fig. 6) and a larger one consisting of 468 polygons (see Fig 12). We highlight two aspects of the efficiency of this modeling

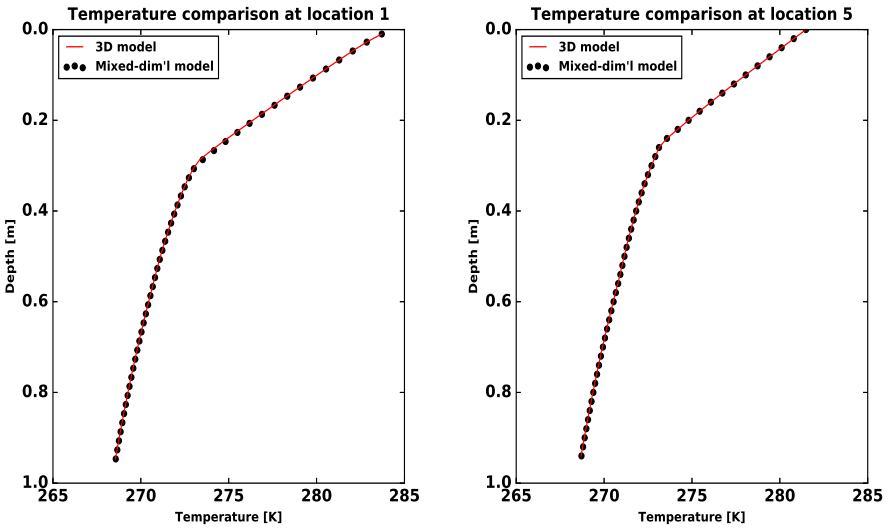

Figure 8: Comparison of subsurface temperature at locations 1 and 5 during the summer. Results correspond to $\alpha = 1$.

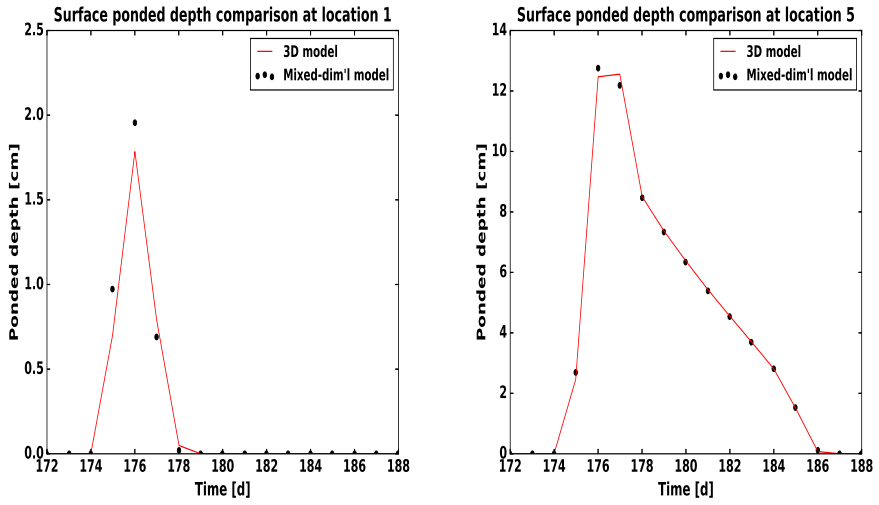

Figure 9: An illustration of the surface ponded depths of the two schemes at locations 1 and 5 during the summer. Results correspond to $\alpha = 1$.

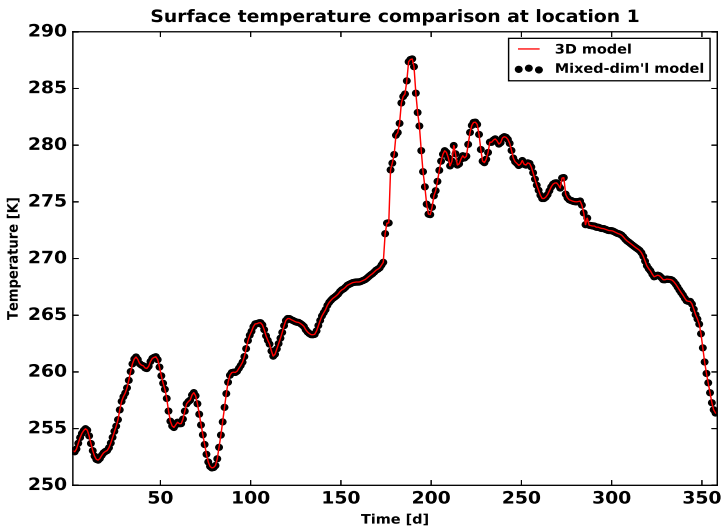

Figure 10: An illustration of the surface temperature of the two schemes at location 1 for the entire year. Results correspond to $\alpha = 1$.

approach: (i) how the simulation time decreases in comparison with three-dimensional simulations, and (ii) how efficiently it scales with number of processes.

Fig. 14 compares the computational time of the multidimensional strategy versus the three-dimensional solution for the domain consisting of 75 columns. It can be seen that for a fixed number of processors, the computational time decreases by a factor of about four with the multidimensional technique. This is a huge computational advantage without sacrificing numerical accuracy.

We show parallel strong scaling for the 468 polygons domain in Fig. 15. Speedup of the 75-polygon domain (not shown) is significantly less than the linear ideal; this is caused by communication overhead in the overland-flow system. Without consideration of the overland-flow system, the problem is

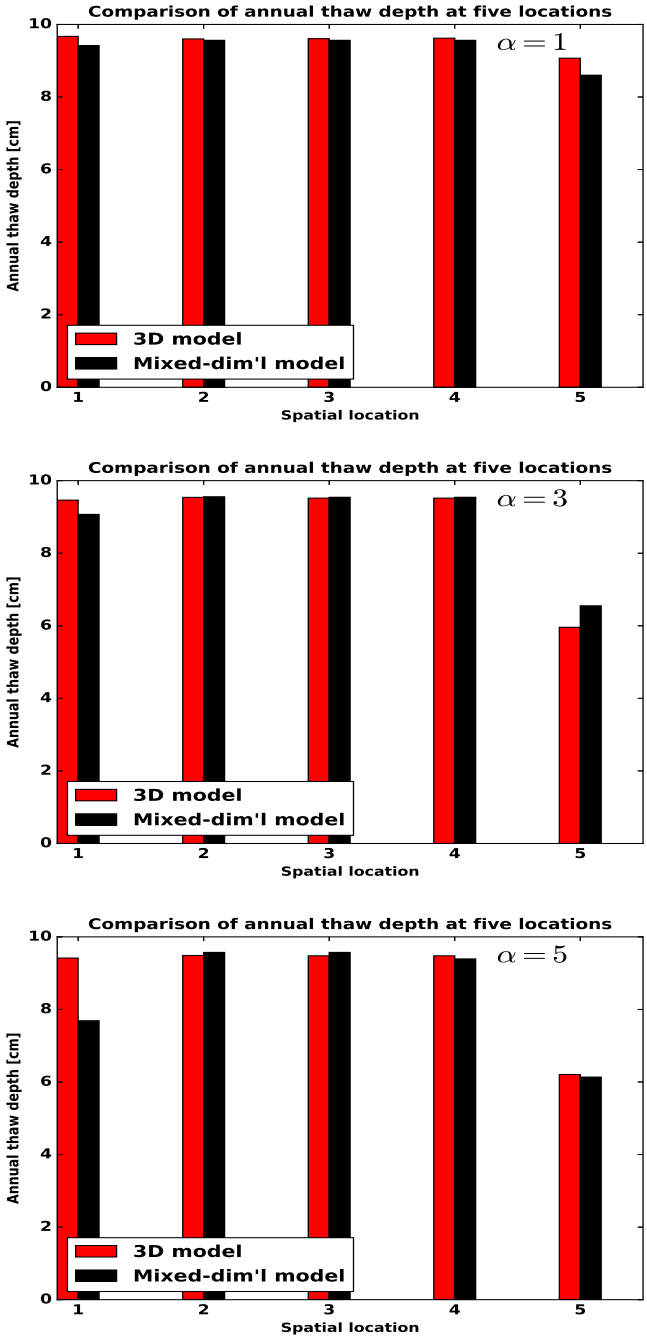

Figure 11: A comparison of the annual thaw depth at the selected locations of the three studies. Results correspond to $\alpha = 1$.

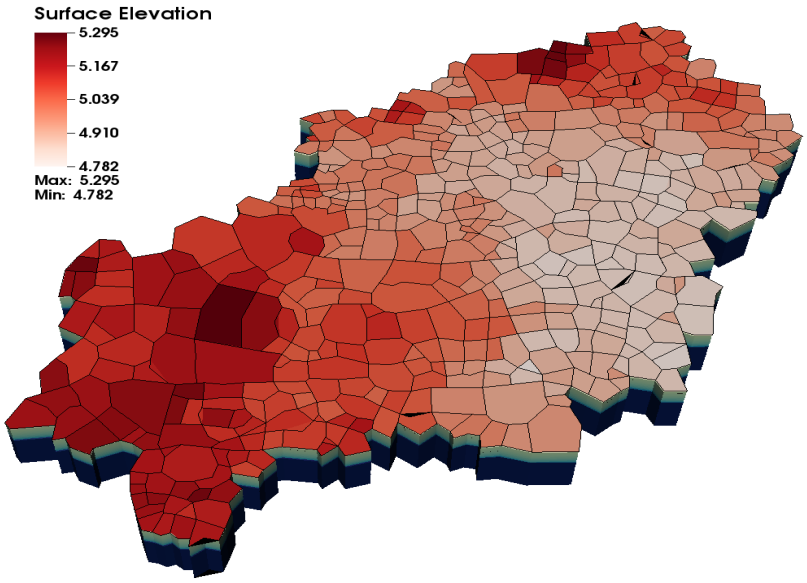

Figure 12: A watershed at Barrow, Alaska.

perfectly parallel. To minimize communication between the overland-flow system and the column systems, the overland-flow mesh is partitioned so that a column and the coincident mesh cells on the overland-flow system reside on the same processor. If there are too few columns per processor, the interprocessor communication for the overland-flow system becomes the limiting factor despite the lower computational burden for the overland-flow system compared with the columns. As expected, the scaling is better for a larger domain. Scaling is close to linear up to about 16 cores, which corresponds to about 30 columns per core.

5.3. Subcycling Process Kernels

One advantage of sequentially coupling different PKs, as opposed to a fully coupled approach, is that sequential coupling makes subcycling possi-

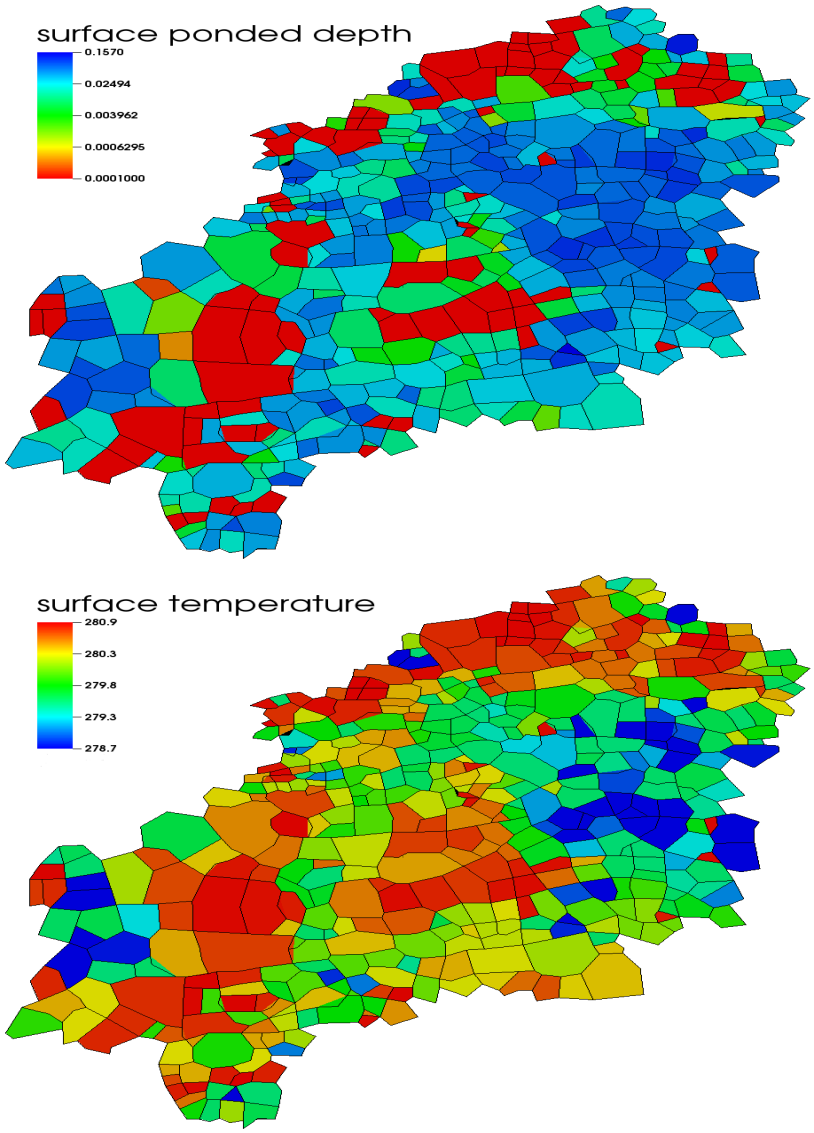

Figure 13: Simulation results from our mixed-dimensional model. Shown are the surface ponded depth and temperature during the snowmelt of 2012. For clarity, the subsurface variables are not shown.

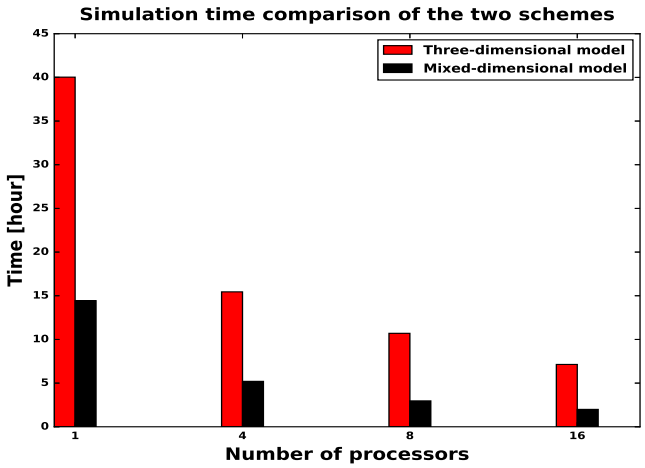

Figure 14: A comparison of the computational time taken by the mixed-dimensional and 3D models.

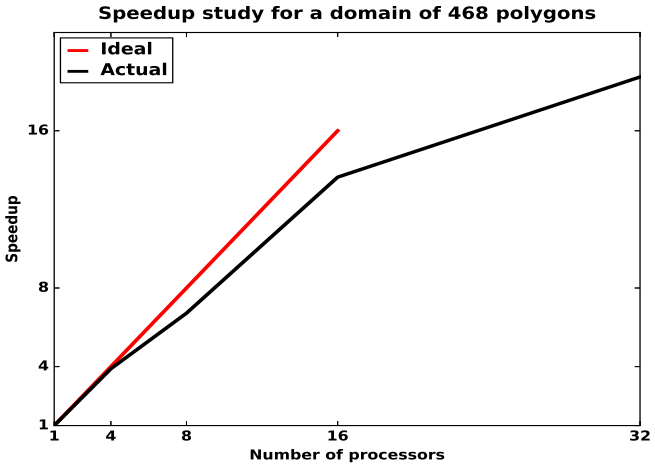

Figure 15: An illustration of the speedup study of a simulation with 468 polygons watershed.

ble. With subcycling, individual PKs take their own time step rather than a global time step. The independently evolving PKs are then synchronized on a larger time step. The idea is to assign a suitable local time-step to each subdomain rather than one single global time-step. It is a very convenient approach for simulating permafrost type regions because a relatively small time step may be required when a cell is going through a phase change. Without subcycling, a timestep failure or small timestep caused by phase change in a single cell results in a small global time step. With subcycling, the effects of that phase transition are limited to a single column. Our mixed-dimensional modeling approach efficiently allows subcycling PKs because we discretize subsurface as independent columns/subdomains. Thus, the subdomains can advance in time with their preferred time-steps until they hit the synchronized time. Fig. 16 displays percentage reduction in the simulation time for the domains consisting of 21, 75, and 468 polygons. With the increase in the number of subsurface columns the computational time decreases, and we see up to 40% reduction in the computational time in comparison with simulations without subcycling. The choice of the synchronization time is crucial, and requires further optimization, which will be studied in future work.

6. Conclusions and Future Work

Our intermediate-scale model for integrated surface/subsurface thermal hydrology of low-relief permafrost-affected regions is constructed from two components: a mixed-dimensional spatial structure that is based on discretizing the subsurface as independent columns that are indirectly coupled through a two-dimensional surface system, and an operator splitting scheme

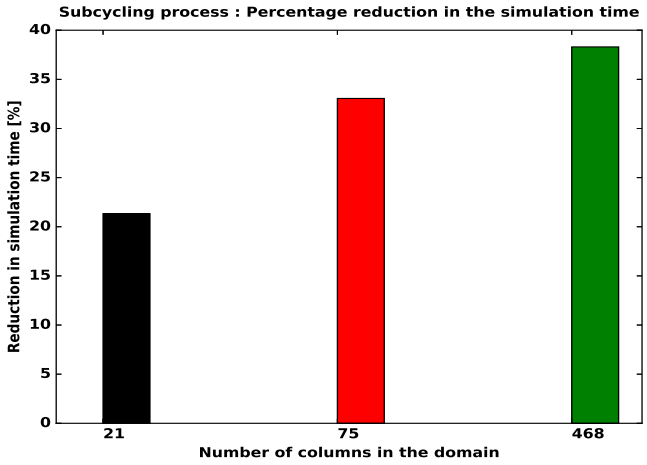

Figure 16: (Subcycling PKs) Percentage reduction in the computational time for the domains consisting of 21, 75 and 468 polygons.

for coupling the column domains to the surface system. The spatial structure was motivated by fine-scale simulations of permafrost regions. This is the first demonstration of advanced representations of freezing soil physics coupled to overland thermal flow and surface energy balance at scales of 100s of meters.

An operator splitting algorithm is used to advance our mixed-dimensional model. First, we solve a two-dimensional surface thermal hydrology system that spatially distributes mass and energy, and initializes the system of the second step. The second step solves a family of independent one-dimensional columns, where each represents an integrated system of the subsurface, surface ponding and surface energy balance. That step updates the 2D surface system of the first step for the next iteration.

We compared our numerical results to the conventional scheme of a fully 3D subsurface that is strongly coupled to a surface system to demonstrate

the efficiency and accuracy of our modeling approach. The fully coupled results act as a benchmark for our scheme. Numerical results show our scheme closely approximates the fully coupled system but is significantly more efficient. The scheme also allows for subcycling of individual subdomains, which further improves the numerical efficiency. With subcycling we see about an order of magnitude improvement in execution time compared to the fully 3D configuration on a 75-polygon mesh. However, we expect the computational advantages to improve with the system size. Indeed, we were not able to run the 468-polygon domain in fully 3D mode due to computational limitations, but were readily able to do it with the mixed-dimensional approximation.

This work is part of a larger effort to provide process-rich, watershed-scale simulations capability for permafrost regions. Given the good scaling properties of our approach, we anticipate that simulations resolving individual ice-wedge polygons are now feasible for domains corresponding to those of a next-generation Earth system model grid cell ($\approx$ 10 km). in addition, the spatial structure used here is applicable at continental scales if a coarser discretization is used, wherein each surface grid cell corresponds to a sub-watershed in a ESM grid cell.

From the model development perspective, an important next step is to incorporate a subgrid model to represent the effects of variations of topography below our discretization unit of the ice wedge polygon. Another future direction is to represent thaw-induced subsidence. Thawing of permafrost and melting of massive subsurface ice can cause differential subsidence, leading to dynamic microtopography (low-centered polygons can transform to high-centered polygons) [48, 49], substantial changes in hydrology and soil moisture, and altered drainage networks, thus potentially transforming a

wetland ecosystem to a dry region [50, 51]. This modeling strategy is designed to tractably represent thaw-induced subsidence. Representing subsidence in one dimension is significantly easier than a fully three-dimensional representation because mesh tangling and other mesh quality issues arise in a fully three-dimensional dynamic mesh but are avoided in one dimension. Indeed, simulations of thaw-induced subsidence on a single one-dimensional integrated surface/subsurface system has already been demonstrated [14]; the work described here will allow the same techniques to be used at scale with many columns coupled to an overland flow system.

Although we mainly focus on simulating the thermal hydrology of degrading permafrost, elements of the work presented here have greater applicability. A hybrid spatial structure mixing one-dimensional representations of the vadose zone with two-dimensional representations of the saturated zone and overland flow system are important approximations in watershed modeling. This operator-split scheme of Fig. 4 is broadly applicable to those systems and to integrated surface/subsurface simulations, in general. This mixed-dimensional representation may be used as an alternative to a fully coupled system or as a way of accelerating the time-consuming task of spinup. In addition, this work demonstrates the advantages of Arcos or other multiphysics management frameworks in greatly simplifies the process of building models with hybrid spatial structure.

Acknowledgments

This work was supported by Interoperable Design of Extreme-scale Application Software (IDEAS) project and by the Next Generation Ecosystem Experiment (NGEE-Arctic) project. NGEE-Arctic is supported by the

Office of Biological and Environmental Research in the DOE Office of Science. We are also grateful to Jitu Kumar, Lauren Charsley-Groffman, Terry Miller, Garrett Altman and Lucia Short for help in constructing computational meshes.

Appendix A. Numerical Experiments – Code Verification

We have performed a series of tests at the development stage for code verification, and compared our results against numerical solution of three-dimensional model. The 3D results serve as a benchmark for our scheme. In 3D models the surface and subsurface systems are strongly coupled and solved implicitly. Since our model required major refactoring of the ATS, so individual pieces of the code were deeply tested before integration – they are listed below:

- Problem Test 1 (Subsurface Flow): We consider multiple subsurface columns with flat top surface – each column is an independent domain. Put water table below the surface, infiltrates and fills the subsurface columns.

- Problem Test 2 (Surface and Subsurface Flow only): This is an extension of the Test 1. We put water table below the surface. Water infiltrates and fill subsurface columns prior to surface ponding.

- Problem Test 3 (Subsurface Thermal Hydrology): We add energy equation to Test 1. Initially, establish water table close to the surface, and start freezing from below. The frozen subsurface columns are thawed from the top.

- Problem Test 4 (Surface and Subsurface Thermal Hydrology): In this test, we incorporate surface thermal hydrology into Test 3. A warm rain precipitation thaws the subsurface columns, saturate them and afterwards water ponds on the surface.

- Problem Test 5 (Surface Energy Balance, Surface and Subsurface Thermal Hydrology): A fully integrated surface and subsurface processes test. We introduce an energy balance equation to Test 4. An initially established ice table below the surface has been thawed by warm rain, incoming-short radiation and air temperature.

Due to symmetry in the domains of above numerical tests, that is, the subsurface columns are copies of each other and surface is flat, we get identical results and compare very well with its corresponding three-dimensional simulation results. Passing all the above tests conclude refactoring of the ATS a success. In the preceding discussion, we consider general polyhedra due to the polygonal structure of the Arctic landscape.

References

[1] J. Brown, O. Ferrians Jr, J. Heginbottom, E. Melnikov, Circum-Arctic map of permafrost and ground-ice conditions, 45, 1997.

[2] M. T. Jorgenson, C. H. Racine, J. C. Walters, T. E. Osterkamp, Permafrost degradation and ecological changes associated with a warming-climate in central alaska, Climatic change 48 (2001) 551–579.

[3] E. A. G. Schuur, A. D. McGuire, C. Schaedel, G. Grosse, J. W. Harden, D. J. Hayes, G. Hugelius, C. D. Koven, P. Kuhry, D. M. Lawrence, S. M. Natali, D. Olefeldt, V. E. Romanovsky, K. Schaefer, M. R. Turetsky,

C. C. Treat, J. E. Vonk, Climate change and the permafrost carbon feedback, NATURE 520 (2015) 171–179.

[4] G. Hugelius, J. Strauss, S. Zubrzycki, J. W. Harden, E. A. G. Schuur, C.-L. Ping, L. Schirrmeister, G. Grosse, G. J. Michaelson, C. D. Koven, J. A. O'Donnell, B. Elberling, U. Mishra, P. Camill, Z. Yu, J. Palmtag, P. Kuhry, Estimated stocks of circumpolar permafrost carbon with quantified uncertainty ranges and identified data gaps, Biogeosciences 11 (2014) 6573–6593.

[5] J. Turner, J. E. Overland, J. E. Walsh, An arctic and antarctic perspective on recent climate change, International Journal of Climatology 27 (2007) 277–293.

[6] J. Hansen, R. Ruedy, J. Glascoe, M. Sato, Giss analysis of surface temperature change, Journal of Geophysical Research: Atmospheres 104 (1999) 30997–31022.

[7] A. C. I. Assessment, Impacts of a warming arctic-arctic climate impact assessment, Impacts of a Warming Arctic-Arctic Climate Impact Assessment, by Arctic Climate Impact Assessment, pp. 144. ISBN 0521617782. Cambridge, UK: Cambridge University Press, December 2004. 1 (2004).

[8] C. D. Koven, B. Ringeval, P. Friedlingstein, P. Ciais, P. Cadule, D. Khvorostyanov, G. Krinner, C. Tarnocai, Permafrost carbon-climate feedbacks accelerate global warming, Proceedings of the National Academy of Sciences 108 (2011) 14769–14774.

[9] T. Osterkamp, Response of alaskan permafrost to climate, in: Fourth

International Conference on Permafrost, Fairbanks, Alaska, 1983, pp. 17–22.

[10] M. A. Walvoord, R. G. Striegl, Increased groundwater to stream discharge from permafrost thawing in the yukon river basin: Potential impacts on lateral export of carbon and nitrogen, Geophysical Research Letters 34 (2007).

[11] S. Lyon, G. Destouni, R. Giesler, C. Humborg, C.-M. Mörth, J. Seibert, J. Karlsson, P. Troch, Estimation of permafrost thawing rates in a subarctic catchment using recession flow analysis, Hydrology and Earth System Sciences 13 (2009) 595–604.

[12] R. K. Pachauri, M. Allen, V. Barros, J. Broome, W. Cramer, R. Christ, J. Church, L. Clarke, Q. Dahe, P. Dasgupta, et al., Climate change 2014: Synthesis report. contribution of working groups i, ii and iii to the fifth assessment report of the intergovernmental panel on climate change (2014).

[13] C. D. Koven, W. J. Riley, A. Stern, Analysis of permafrost thermal dynamics and response to climate change in the CMIP5 earth system models, Journal of Climate 26 (2013) 1877–1900.

[14] S. Painter, J. Moulton, C. Wilson, Modeling challenges for predicting hydrologic response to degrading permafrost, Hydrogeology Journal (2013) 1–4.

[15] B. L. Kurylyk, K. T. MacQuarrie, J. M. McKenzie, Climate change impacts on groundwater and soil temperatures in cold and temperate

regions: Implications, mathematical theory, and emerging simulation tools, Earth-Science Reviews 138 (2014) 313–334.

[16] R. Harlan, Analysis of coupled heat-fluid transport in partially frozen soil, Water Resources Research 9 (1973) 1314–1323.

[17] G. L. Guymon, J. N. Luthin, A coupled heat and moisture transport model for arctic soils, Water Resources Research 10 (1974) 995–1001.

[18] G. S. Taylor, J. N. Luthin, A model for coupled heat and moisture transfer during soil freezing, Canadian Geotechnical Journal 15 (1978) 548–555.

[19] K. Takata, S. Emori, T. Watanabe, Development of the minimal advanced treatments of surface interaction and runoff, Global and planetary Change 38 (2003) 209–222.

[20] D. Nicolsky, V. Romanovsky, V. Alexeev, D. Lawrence, Improved modeling of permafrost dynamics in a gcm land-surface scheme, Geophysical research letters 34 (2007).

[21] D. M. Lawrence, A. G. Slater, S. C. Swenson, Simulation of present-day and future permafrost and seasonally frozen ground conditions in ccsm4, Journal of Climate 25 (2012) 2207–2225.

[22] J. M. McKenzie, C. I. Voss, D. I. Siegel, Groundwater flow with energy transport and water–ice phase change: numerical simulations, benchmarks, and application to freezing in peat bogs, Advances in water resources 30 (2007) 966–983.

[23] V. Bense, G. Ferguson, H. Kooi, Evolution of shallow groundwater flow

systems in areas of degrading permafrost, Geophysical Research Letters 36 (2009).

[24] S. L. Painter, S. Karra, Constitutive model for unfrozen water content in subfreezing unsaturated soils, Vadose Zone Journal 13 (2014).

[25] S. L. Painter, Three-phase numerical model of water migration in partially frozen geological media: model formulation, validation, and applications, Computational Geosciences 15 (2011) 69–85.

[26] R. E. Grimm, S. L. Painter, On the secular evolution of groundwater on mars, Geophysical Research Letters 36 (2009) n/a–n/a. L24803.

[27] A. Frampton, S. Painter, S. W. Lyon, G. Destouni, Non-isothermal, three-phase simulations of near-surface flows in a model permafrost system under seasonal variability and climate change, Journal of Hydrology 403 (2011) 352 – 359.

[28] S. Karra, S. Painter, P. Lichtner, Three-phase numerical model for subsurface hydrology in permafrost-affected regions, Cryosphere Discuss 8 (2014) 149–185.

[29] P. C. Lichtner, G. E. Hammond, C. Lu, S. Karra, G. Bisht, B. Andre, R. T. Mills, J. Kumar, PFLOTRAN Web page, 2013. Http://www.pflotran.org.

[30] J. Kumar, N. Collier, G. Bisht, R. T. Mills, P. E. Thornton, C. M. Iversen, V. Romanovsky, Modeling the spatiotemporal variability in subsurface thermal regimes across a low-relief polygonal tundra landscape, The Cryosphere 10 (2016) 2241–2274.

[31] S. L. Painter, E. T. Coon, A. L. Atchley, M. Berndt, R. Garimella, J. D. Moulton, D. Svyatskiy, C. J. Wilson, Integrated surface/subsurface permafrost thermal hydrology: Model formulation and proof-of-concept simulations, Water Resources Research 52 (2016) 6062–6077.

[32] E. T. Coon, J. D. Moulton, S. L. Painter, Managing complexity in simulations of land surface and near-surface processes, Environmental Modelling & Software 78 (2016) 134–149.

[33] M. Dall'Amico, S. Endrizzi, S. Gruber, R. Rigon, A robust and energy-conserving model of freezing variably-saturated soil, The Cryosphere 5 (2011) 469–484.

[34] M. F. Pikul, R. L. Street, I. Remson, A numerical model based on coupled one-dimensional richards and boussinesq equations, Water Resources Research 10 (1974) 295–302.

[35] Y. Zhu, Y. Zha, J. Tong, J. Yang, Method of coupling 1-d unsaturated flow with 3-d saturated flow on large scale, Water Science and Engineering 4 (2011) 357–373.

[36] P. Hazenberg, Y. Fang, P. Broxton, D. Gochis, G.-Y. Niu, J. D. Pelletier, P. A. Troch, X. Zeng, A hybrid-3d hillslope hydrological model for use in earth system models, Water Resources Research 51 (2015) 8218–8239.

[37] E. T. Coon, ATS: The Advanced Terrestrial Simulator, 2016. http://github.com/amanzi/ats.

[38] J. D. Moulton, M. Berndt, R. Garimella, L. Prichett-Sheats, G. Hammond, M. Day, J. Meza, High-level design of amanzi, the multi-process

high performance computing simulator, office of environmental management, united states department of energy, washington dc (2012).

[39] M. Heroux, R. Bartlett, V. H. Hoekstra, J. Hu, T. Kolda, R. Lehoucq, K. Long, R. Pawlowski, E. Phipps, A. Salinger, H. Thornquist, R. Tuminaro, J. Wil-lenbring, A. Williams, An overview of trilinos. Technical report sand2003-2927, Sandia National Laboratory (2003).

[40] R. V. Garimella, W. A. Perkins, M. W. Buksas, M. Berndt, K. Lipnikov, E. Coon, J. D. Moulton, S. L. Painter, Mesh infrastructure for coupled multiprocess geophysical simulations, Procedia Engineering 82 (2014) 34 – 45.

[41] L. B. da Veiga, K. Lipnikov, G. Manzini, The mimetic finite difference method for elliptic problems, volume 11, Springer, 2014.

[42] K. Lipnikov, G. Manzini, M. Shashkov, Mimetic finite difference method, Journal of Computational Physics 257 (2014) 1163–1227.

[43] M. T. Calef, E. D. Fichtl, J. S. Warsa, M. Berndt, N. N. Carlson, Nonlinear krylov acceleration applied to a discrete ordinates formulation of the k-eigenvalue problem, Journal of Computational Physics 238 (2013) 188–209.

[44] N. N. Carlson, K. Miller, Design and application of a gradient-weighted moving finite element code i: in one dimension, SIAM Journal on Scientific Computing 19 (1998) 728–765.

[45] A. L. Atchley, S. L. Painter, D. R. Harp, E. T. Coon, C. J. Wilson, A. K. Liljedahl, V. E. Romanovsky, Using field observations to inform

thermal hydrology models of permafrost dynamics with ats (v0.83), Geoscientific Model Development 8 (2015) 2701–2722.

[46] A. L. Atchley, E. T. Coon, S. L. Painter, D. R. Harp, C. J. Wilson, Influences and interactions of inundation, peat, and snow on active layer thickness, Geophysical Research Letters 43 (2016) 5116–5123. 2016GL068550.

[47] Lawrence Livermore National Laboratory, A mesh and field i/o library and scientific database, 2016. Https://wci.llnl.gov/simulation/computer-codes/silo.

[48] M. T. Jorgenson, Y. L. Shur, E. R. Pullman, Abrupt increase in permafrost degradation in arctic alaska, Geophysical Research Letters 33 (2006).

[49] A. Liljedahl, L. Hinzman, J. Schulla, Ice-wedge polygon type controls low-gradient watershed-scale hydrology, in: Proceedings of the Tenth International Conference on Permafrost, volume 1, 2012, pp. 231–236.

[50] L. D. Hinzman, N. D. Bettez, W. R. Bolton, F. S. Chapin, M. B. Dyurgerov, C. L. Fastie, B. Griffith, R. D. Hollister, A. Hope, H. P. Huntington, et al., Evidence and implications of recent climate change in northern alaska and other arctic regions, Climatic Change 72 (2005) 251–298.

[51] J. C. Rowland, C. E. Jones, G. Altmann, R. Bryan, B. T. Crosby, L. D. Hinzman, D. L. Kane, D. M. Lawrence, A. Mancino, P. Marsh, J. P. McNamara, V. E. Romanvosky, H. Toniolo, B. J. Travis, E. Trochim, C. J. Wilson, G. L. Geernaert, Arctic landscapes in transition: Responses to

thawing permafrost, Eos, Transactions American Geophysical Union 91 (2010) 229–230.